THE JOURNAL OF PHYSICAL CHEMISTRY A

ARTICLE

pubs.acs.org/JPCA

Synthesis, Characterization, and Spectroscopic Investigation of Benzoxazole Conjugated Schiff Bases

Fabiano S. Santos,[†,‡] Tania M. H. Costa,[†] Valter Stefani,[‡] Paulo F. B. Gonçalves,[§] Rodrigo R. Descalzo,[§] Edilson V. Benvenutti,[*,†] and Fabiano S. Rodembusch[*,‡]

[†]Laboratório de Sólidos e Superfícies, [‡]Laboratório de Novos Materiais Orgânicos, and [§]Grupo de Química Teórica e Computacional, Universidade Federal do Rio Grande do Sul - Instituto de Química, Avenida Bento Gonçalves, 9500, CP 15003, CEP 91501-970 Porto Alegre-RS, Brazil

Supporting Information

ABSTRACT: Two Schiff bases were synthesized by reaction of 2-(4′-aminophenyl)benzoxazole derivatives with 4-*N*,*N*-diethylaminobenzaldehyde. UV−visible (UV−vis) and steady-state fluorescence in solution were applied in order to characterize its photophysical behavior. The Schiff bases present absorption in the UV region with fluorescence emission in the blue-green region, with a large Stokes' shift. The UV−vis data indicates that each dye behaves as two different chromophores in solution in the ground state. The fluorescence emission spectra of the dye **5a** show that an intramolecular proton transfer (ESIPT) mechanism takes place in the excited state, whereas a twisted internal charge transfer (TICT) state is observed for the dye **5b**. Theoretical calculations were performed in order to study the conformation and polarity of the molecules at their ground and excited electronic states. Using density functional theory (DFT) methods at theoretical levels BLYP/Aug-SV(P) for geometry optimizations and B3LYP/6-311++G(2d,p) for single-point energy evaluations, the calculations indicate that the lowest energy conformations are in all cases nonplanar and that the dipole moments of the excited state relaxed structures are much larger than those of the ground state structures, which corroborates the experimental UV−vis absorption results.

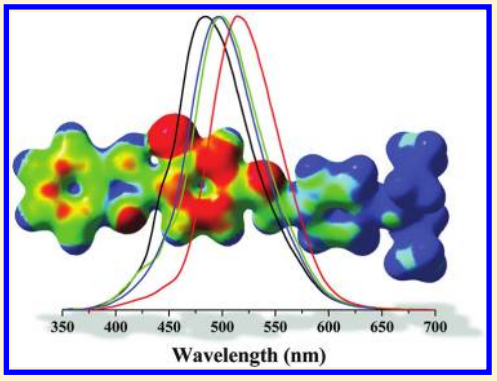

INTRODUCTION

The growth of the world energy demand, as well as the search for renewable energy sources that do not cause expressive damage to the environment has led chemists to look for new devices that can take advantage of solar radiation with larger efficiency, increasing the contribution of renewable sources of energy.[1−3] Solar energy is highlighted due to its enormous availability,[4] as well as it being directly converted into electricity by exploration of the photovoltaic effect.[5−8] Photovoltaic devices, particularly photoelectrochemical solar cells, such as the Grätzel solar cell,[9−13] take advantage of luminous energy to promote oxireduction reactions using a dye-sensitized solar cell (DSSC).[14−16] Several photoactive structures have been used as fluorescent sensitizers, such as coumarin and merocyanines.[17−25] In this context, benzazole dyes can potentially be applied as DSSC dyes, due to their well-know phototautomerism in the excited state (ESIPT),[26−28] which allows higher photochemical and photothermal stability.[29] In the ESIPT mechanism, the light absorption by an enol conformer produces an excited enol, which is quickly converted to an excited keto tautomer by an intramolecular proton transfer. The excited keto tautomer decays, emitting fluorescence to a keto tautomer in the ground state. Since the enol conformer is more stable than the keto tautomer in the ground state, the initial enol form is regenerated without any photochemical change. On the other hand, donor−acceptor fluorescent molecules based on benzazoles have been described in the literature,[30−32] where an internal charge transfer (ICT) state[33−36] takes place on the excited state. Additionally, it is desirable for a DSSC dye to present energy absorption in the visible region, since in a Grätzel cell the semiconductor oxide film TiO_2 presents absorption in the UV region. In order to satisfy this requirement using benzazole dyes, its conjugation must be extended, as for instance in a Schiff base structure. In this way, this work presents the synthesis, characterization, and photophysical study of novel Schiff bases with electronic structures similar to those observed in DSSC dyes.

EXPERIMENTAL SECTION

Materials and Methods. All the solvents and reagents were used as received or purified using standard procedures. Spectroscopic-grade solvents (Merck) were used for fluorescence and UV−visible (UV−vis) measurements. Elemental analyses were performed by a Perkin-Elmer model 240. Melting points were

Received: July 19, 2011
Revised: October 6, 2011
Published: October 11, 2011

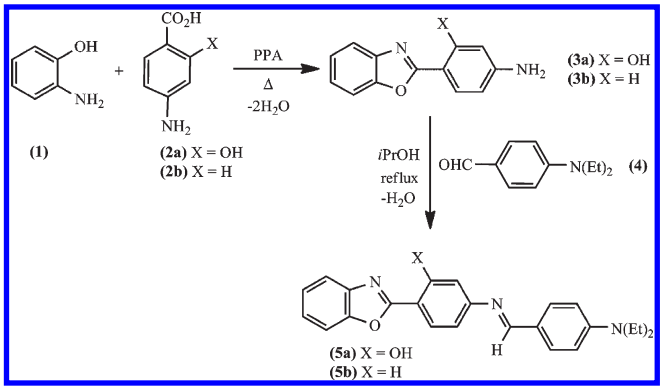

Figure 1. Synthesis of the Schiff bases **5a,b**.

measured with a Gehaka PF 1000 apparatus and are uncorrected. Infrared spectra were recorded on a Shimadzu Prestige 21 in ATR mode. ^{1}H and ^{13}C NMR spectra were performed on a VARIAN INOVA YH300 using tetramethylsilane (TMS) as the internal standard and $CDCl_3$ and DMSO-d_6 (Aldrich) as the solvent at room temperature. UV−vis absorption spectra were performed on a Shimadzu UV-2450 spectrophotometer. Steady-state fluorescence spectra were measured with a Shimadzu spectrofluorometer model RF-5301PC. Spectrum correction was performed to enable measuring a true spectrum by eliminating instrumental response such as wavelength characteristics of the monochromator or detector using Rhodamine B as a standard (quantum counter). All experiments were performed at room temperature at a concentration of 10^{-5} M.

Theoretical Calculations. The theoretical calculations were performed using Orca 2.8 software[37] at the BLYP/Aug-SV(P) level and also using Gaussian 03 software[38] at the B3LYP/6-311++G(2d,p) level of theory. The ground electronic state conformation and properties of structures **5a**(enol) and **5b** were obtained by first optimizing the geometry of the ground state of each species using the BLYP pure functional (with RI-J approximation) together with the Aug-SV(P) basis set in Orca 2.8, and subsequently performing a single-point energy calculation at their optimized geometries using the B3LYP hybrid functional together with the 6-311G(2d,p) basis set in Gaussian 03. The excited electronic state conformation and properties of structures **5a**(enol conformer), **5a**(keto tautomer), and **5b** were similarly obtained. For each of the three species, the methodology was as follows: The first step was to perform a pure time-dependent density functional theory (TD-DFT) energy calculation of the ground state optimized structure (as obtained above) in order to determine which was the most probable excited state for the current species; after that, the selected excited state had its geometry optimized. Both steps were run using Orca at the level of theory mentioned above, BLYP/Aug-SV(P). The final step was to perform a hybrid TD-DFT energy calculation of the optimized structure for the excited state obtained in the previous step. The output data corresponding to the most probable excited state as indicated by the oscillator strengths of this final calculation, which was run using Gaussian at the B3LYP/6-311++G(2d,p) level, was selected. Onsager radii were calculated using the polarizable continuum model as the self-consistent reaction field method in Gaussian.

Synthesis of the Schiff Bases. The dyes **3a,b** were prepared using a methodology previously described (spectroscopic data available in the Supporting Information).[39] The Schiff bases **5a,b**

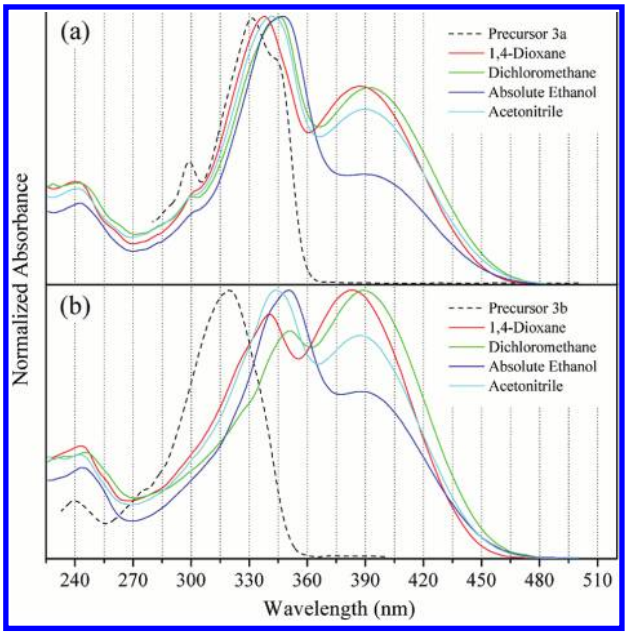

Figure 2. Normalized absorption spectra of the Schiff base **5a** (a) and **5b** (b). The precursors in dichloromethane are also presented for comparison (dotted line).[40]

were prepared according to Figure 1. In a typical experiment, an equimolar amount of the amino derivative **3a,b** and 4-*N*,*N*-diethylaminobenzaldehyde (**4**) was stirred under reflux for 4 h. The product, which precipitates in the reaction media, was filtered and washed with cold isopropanol several times and dried at room temperature.

*(E) N,N-Diethyl-4-[4′-(benzoxazolyl)-3′-hydroxyphenyl]-benzylideneimine (**5a**).* Yield: 87%; mp: > 200 °C. IR (ATR, cm^{-1}): 3081 and 3055 (νCH arom.), 2970, 2925, and 2866 (νCH aliphatic), 1633 (νC═C arom.), 1585 (νC═N imino), 1487 (νC═C arom.). ^{1}H NMR (300 MHz, $CDCl_3$): δ (ppm) = 11.53 (broad s, 1H, OH), 8.31 (s, 1H, CH imine), 7.98 (d, J_o = 8.3 Hz, 1H, H_A), 7.75 (d, J_o = 8.6 Hz, 2H, H_B), 7.67−7.70 (m, 1H, H_7), 7.56−7.58 (m, 1H, H_1), 7.33−7.36 (m, 2H, H_5 and H_6), 6.84 (dd, J_o = 8.3 Hz, J_m = 1.76 Hz, 1H, H_B), 6.69 (d, J_o = 8.6 Hz, 2H, H_{B1}), 6.68 (s, 1H, H_X), 3.42 (q, 4H, CH_2), 1.20 (t, 6H, CH_3). ^{13}C NMR (75.4 MHz, $CDCl_3$): δ (ppm) = 163.1; 160.9; 159.6; 158.1; 150.4; 148.9; 140.1; 131.1; 127.7; 124.9; 124.7; 123.0; 118.8; 113.8; 110.9; 110.4; 108.6; 107.1; 44.5; 12.5. Anal. Calcd. for $C_{24}H_{23}N_3O_2$ (385.46 g·mol^{-1}): C: 74.78; H: 6.01; N: 10.90. Found: C: 72.97; H: 5.89; N: 10.37. EIMS: m/z (%) = 385.20 [M^+] (60), 370.15 (100).

*(E) N,N-Diethyl-4-[4′-(benzoxazolyl)]benzylideneimine (**5b**).* Yield: 88%; mp: > 200 °C. IR (ATR, cm^{-1}): 3075 and 3020 (νCH arom.), 2967, 2931, and 2888 (νCH aliphatic), 1621 (νC═C arom.), 1602 (νC═N imino), 1486 (νC═C arom.). ^{1}H NMR (300 MHz, $CDCl_3$): δ (ppm) = 8.34 (s, 1H, CH imine), 8.25 (d, J_o = 8.6 Hz, 2H, H_{B2}), 7.77 (d, J_o = 8.9 Hz, 2H, H_{A1}), 7.74−7.76 (m, 1H, H_1), 7.58−7.55 (m, 1H, H_1), 7.35−7.32 (m, 4H, H_2, H_3 and H_{A2}), 6.69 (d, J_o = 8.9 Hz, 2H, H_{B1}), 3.43 (q, 4H, CH_2), 1.21 (t, 6H, CH_3). ^{13}C NMR (75.4 MHz, $CDCl_3$): δ (ppm) = 163.2, 160.8, 155.9, 150, 142.2, 131, 128.6, 124.7, 124.4, 123, 121.5, 119.6, 114.5, 110.9, 110.4, 44.5, 12.5. Anal. Calcd. for $C_{24}H_{23}N_3O_2$ (369.46 g·mol^{-1}): C; 78.02; H: 6.27; N: 11.37. Found: C: 76.71; H: 6.49; N: 10.78. EIMS: m/z (%) = 369.12 [M^+] (61), 354.15 (100).

dx.doi.org/10.1021/jp206905f |*J. Phys. Chem. A* 2011, 115, 13390–13398

Table 1. Relevant UV−Vis Data of the Schiff Bases in Different Solvents

dye	solvent	LW (nm/eV)	$\varepsilon \times 10^4$ ($l \cdot mol^{-1} \cdot cm^{-1}$)	SW (nm/eV)	$\varepsilon \times 10^4$ ($l \cdot mol^{-1} \cdot cm^{-1}$)
5a	1,4-dioxane	387/3.20	5.6	338/3.67	7.2
	dichloromethane	392/3.16	3.0	345/3.59	3.7
	absolute ethanol	389/3.19	1.9	348/3.56	3.2
	acetonitrile	390/3.18	3.0	342/3.63	5.6
5b	1,4-dioxane	383/3.24	5.0	340/3.65	3.2
	dichloromethane	388/3.20	5.0	351/3.53	4.5
	absolute ethanol	389/3.19	2.8	351/3.53	3.9
	acetonitrile	387/3.20	2.4	344/3.60	3.0

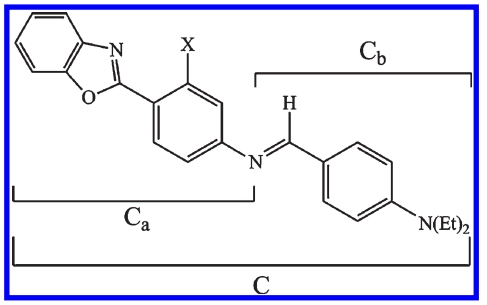

Figure 3. Proposed chromophores in nonplanar Schiff bases, where X = OH or H.

RESULTS

UV−Vis Absorption. In Figure 2a,b are presented the normalized UV−vis absorption spectra of the Schiff bases **5a**-**b**, respectively in 1,4-dioxane, dichloromethane, absolute ethanol, and acetonitrile. The relevant UV−vis data are summarized in Table 1.

An absorption band maxima, the so-called long wavelength (LW), located around 389 nm with molar extinction coefficient values (ε) in agreement with $\pi-\pi^*$ transitions, can be observed for the dye **5a** (Figure 2a). A more intense blue-shifted band, the so-called short wavelength (SW), can be observed located at 343 nm, and is also ascribed to $\pi-\pi^*$ transitions. A positive solvatochromic effect can be observed for this dye (5−10 nm). The difference in the intensities of the absorption bands can be related to a difference of planarity of the different chromophores present in the dye,[28,41] where a nonplanar structure does not allow a more effective electronic delocalization among the three π systems. In this way, for these structures it can be discussed in terms of Schiff, benzoxazolic, and diethylamino chromophores, denoted as C, C_a, and C_b, respectively (Figure 3). The Schiff chromophores (C) would be responsible for the LW absorption bands, and the benzoxazolic chromophore (C_a) is related to the SW bands. The observed difference between the molecular planarity of this dye is confirmed taking into account the molar extinction coefficient values. A less planar structure usually presents a lower probability for the $\pi-\pi^*$ transition, as observed in this dye. Additionally, as already observed with similar ESIPT dyes,[28,42,43] the benzoxazolyl moiety can present a conformational equilibrium in solution in the ground state, confirmed by the solvatochromic effect presented in the UV−vis spectra.

For the dye **5b** (Figure 2b), both absorption bands (LW and SW) can be observed. However, for this dye, the absorption band intensities seem to be tailored by the solvent polarity. In less polar media (1,4-dioxane and dichloromethane), the LW band, located around 387 nm, is more intense. However, in more polar solvents (absolute ethanol and acetonitrile), the more intense band is the SW one located at 346 nm. The molar extinction coefficient values for both bands are in agreement with $\pi-\pi^*$ transitions. Concerning the UV−vis absorption band intensities from the two dyes, it can be observed that the hydroxyl group in the benzoxazolyl chromophore **5a** plays a fundamental role in the benzoxazolic chromophores (C_a) through its intramolecular hydrogen bond. Once a hydrogen bond is present in the dye structure, the benzoxazolyl chromophore will be more planar than the whole molecule in solution in the ground state. For the dye **5b**, the planarity seems to be dependent on the solvent polarity. Additionally, a more intense positive solvatochromic effect can be observed for this dye (10−12 nm) in relation to **5a**, indicating that the absence of the hydroxyl group allows a more effective electronic delocalization, where a higher push−pull character can be observed between the benzoxazolic ring and the imino moiety, respectively, in the ground state. The electrostatic potential surfaces of these dyes (Figure 9a and Supporting Information Figure SI 25) obtained by theoretical calculations corroborates with this result and will be discussed later.

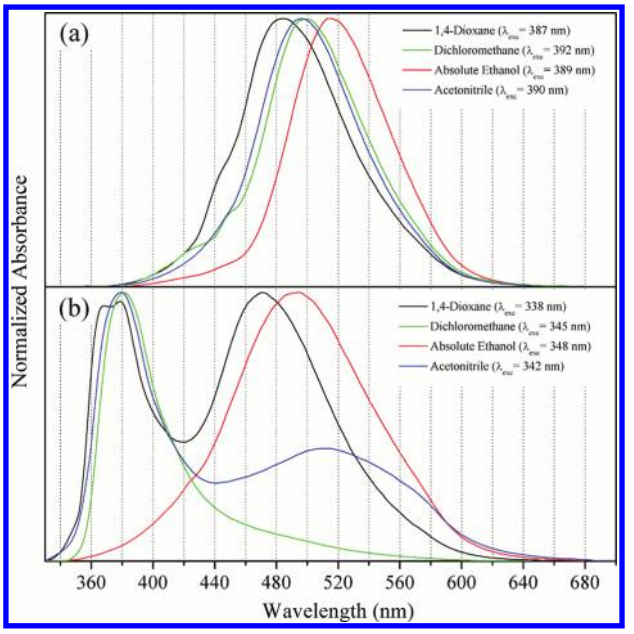

Figure 4. Normalized fluorescence emission of **5a** using (a) LW as the excitation wavelength (387−392 nm) and (b) SW as the excitation wavelength (338−348 nm).

Table 2. Relevant Data from the Fluorescence Emission Curves of the Dye 5a[a]

solvent	LW (nm/eV)	(λ_{em}^{enol}) (nm/eV)	(λ_{em}^{keto}) (nm/eV)	$(\Delta\lambda_{ST})_{enol}$ (nm/eV)	$(\Delta\lambda_{ST})_{keto}$ (nm/eV)
1,4-dioxane	387/3.20		484/2.56		97/0.64
dichloromethane	392/3.16		500/2.48		108/0.68
absolute ethanol	389/3.19		497/2.08		108/1.11
acetonitrile	390/3.18		515/2.41		125/0.77
solvent	SW (nm/eV)	(λ_{em}^{enol}) (nm/eV)	(λ_{em}^{keto}) (nm/eV)	$(\Delta\lambda_{ST})_{enol}$ (nm/eV)	$(\Delta\lambda_{ST})_{keto}$ (nm/eV)
1,4-dioxane	338/3.67	373/3.32	470/2.64	35/0.35	132/1.03
dichloromethane	345/3.59		492/2.52		147/1.07
absolute ethanol	348/3.56	381/3.25	480/2.58	33/0.31	132/0.98
acetonitrile	342/3.63	378/3.21	512/2.42	36/0.42	170/1.21

[a] The first and second sets of data were obtained using LW and SW from the UV−vis curves as excitation wavelengths, respectively.

Although there is a significative shift between the absorption maxima from precursor **3b** and the SW bands from dye **5b** (Figure 2b), we believe that these bands located at 340−351 nm can be ascribed as the chromophore C_a in the dye **5b**. For this statement, we are assuming that (i) a comparison can be made between isolated precursors with chromophores inside the Schiff base structure, which are moderately similar to each other (**3a**/**5a** and **3b**/**5b**); (ii) the isolated precursors present different absorption maxima (Tables SI 1 and SI 2), since the absence of the hydroxyl group in an aromatic ring can blue shift the absorption maxima up to 60 nm;[44,45] (iii) after conjugation (precursor's derivatization), the chromophores present very similar absorption regions, which are red-shifted from the precursors, as expected.[46,47] The obtained data indicates that the precursor's derivatization changes the electronic distribution of the benzoxazole chromophore (C_a) showing that now the hydroxyl group does not play a fundamental role in the electronic distribution in the chromophore (contrary to what was observed for the precursors), since **5a** and **5b** present SW bands in very similar regions. In this way, considering that the SW bands from **5a** and **5b** are in similar regions (due to the respective chromophores), and that the precursor **3b** presents a blue-shifted absorption maxima (in spite of the precursor **3a**), it was expected to observe a higher shift between **3b** and **5b** than **3a** and **5a**.

Fluorescence Emission and Excitation Spectra. Different organic solvents with a wide range of dielectric constants were used in the photophysical characterization of the Schiff bases (Figure 4a,b). The emission spectra were obtained using the LW maxima (387−392 nm), as well as the SW maxima (338−348 nm), respectively. In Table 2 are summarized the relevant data from this photophysical study. In Figure 4a, a main emission band located around 500 nm can be observed, with a relevant solvatochromic effect (∼31 nm), which probably indicates that the dipole moment of the dyes are higher in the excited state than in the ground state. An excitation at the LW means that the fully planar dye is responsible for the absorption followed by fluorescence emission with large Stokes shift. The molecular structure of the dye, as well as the large Stokes shift (∼100 nm) probably indicates that a phototautomerism (ESIPT) takes place in the excited state. The Supporting Information depicts a general scheme (Figure SI 15) of the ESIPT mechanism in the dye **5a**, where an excited keto tautomer (K*), which arises from a totally planar enol conformer (E_I) in the excited state, is responsible for the fluorescence emission with large Stokes shift.[27,28]

In Figure 4b are depicted the emission curves to the dye **5a** using the SW maxima (338−348 nm) as the excitation wavelength. One main fluorescence emission band can be observed in dichloromethane under excitation at 345 nm, which leads to the stabilization of the more planar structure (higher conjugation) in the excited sate. The data presented in the literature indicate that the precursor **3a** presents an emission ascribed to the ESIPT mechanism located at lower wavelengths in comparison to their Schiff base **5a**.[28] In this way, the fluorescence emission observed for this dye in all studied solvents is due to a more planar structure, the so-called Schiff chromophore (C), which excludes the additional chromophores (Figure 3). On the other hand, a particular photophysical behavior can be observed, characterized by a dual fluorescence emission in 1,4-dioxane, absolute ethanol, and acetonitrile. In these solvents, a red-shifted band is present (470−512 nm), ascribed to the ESIPT band and a blue-shifted one (373−381 nm) related to the normal emisson.[28] Usually, the dual fluorescence emission presents a band at higher wavelengths attributed to the excited keto tautomer (K), and a blue-shifted one due to the conformational forms, which are stabilized in solution and present normal

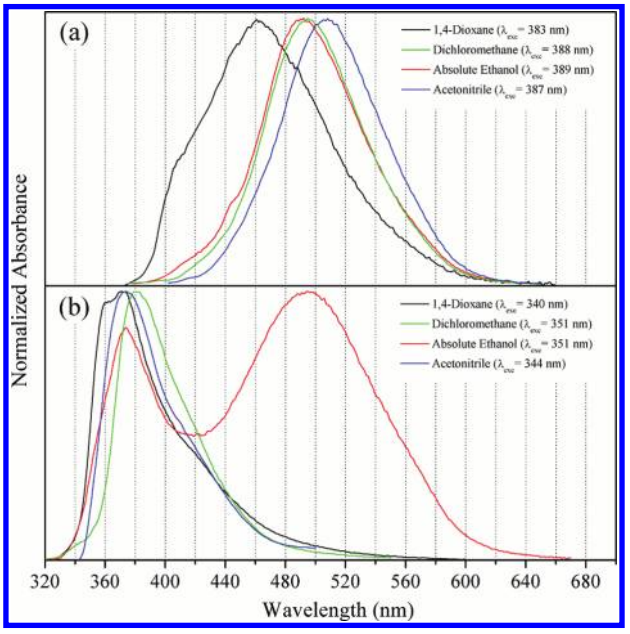

Figure 5. Normalized fluorescence emission of **5b** using (a) LW as the excitation wavelength (383−389 nm) and (b) SW as the excitation wavelengths (340−351 nm).

Table 3. Relevant Data from the Fluorescence Emission Curves of the Dye 5b[a]

solvent	LW(nm/eV)	(λ_{em}^{LE}) (nm/eV)	(λ_{em}^{ICT}) (nm/eV)	$(\Delta\lambda_{ST})_{LE}$ (nm/eV)	$(\Delta\lambda_{ST})_{ICT}$ (nm/eV)
1,4-dioxane	383/3.24		462/2.68		78/0.58
dichloromethane	388/3.20		491/2.53		103/0.67
absolute ethanol	389/3.19		495/2.50		106/0.69
acetonitrile	387/3.20		507/2.45		120/0.75
solvent	SW(nm/eV)	(λ_{em}^{LE}) (nm/eV)	(λ_{em}^{ICT}) (nm/eV)	$(\Delta\lambda_{ST})_{LE}$ (nm/eV)	$(\Delta\lambda_{ST})_{ICT}$ (nm/eV)
1,4-dioxane	340/3.65	368/3.37		28/0.28	
dichloromethane	351/3.53	374/3.32	494/2.51	23/0.21	143/1.02
absolute ethanol	351/3.53	381/3.25		30/0.28	
acetonitrile	344/3.60	375/3.31		31/0.29	

[a] The first and second set of data was obtained using LW and SW from the UV−vis curves as excitation wavelengths, respectively.

relaxation (E_{II-III}).[27,28] Although it is well known that the lower wavelength emissions are due to normal enol conformers, it is worth mentioning that the blue-shifted bands are related to the twisted Schiff bases (benzoxazole chromophore), since the emission values must be higher than the absorption ones (Stoke's law).

In order to confirm the presence of conformers in solution in the ground state, the fluorescence excitation spectra of the dyes were recorded at their enol and/or keto fluorescence emission wavelengths (Figure SI 16). It could be observed for the dye **5a** in 1,4-dioxane, absolute ethanol, and acetonitrile that the excitations at the enol band and the ESIPT band give two distinct spectra. This indicates that the two fluorescence bands originate from at least two different conformers in the ground state, and the absorption spectra of this dye is a mixture of these conformers in the ground state. In dichloromethane, only one band can be observed, probably due to the conformer E_I, which corroborates the main emission band in the fluorescence emission spectra.

The same photophysical study was performed for the dye **5b**, where the fluorescence emission spectra were obtained using the LW maxima (383−389 nm), as well as the SW band (340−351 nm), respectively, and are presented in Figure 5a,b. Table 3 summarizes the relevant data from this photophysical study. One main fluorescence emission band can be observed in all solvents under excitation at LW, which leads to the stabilization of the Schiff chromophore (higher conjugation) in the excited sate. Increasing the solvent polarity, the fluorescence maxima shift from 462 up to 507 nm with a relevant solvatochromic effect (~45 nm) (Figure 5a). Such solvatochromic shifts in the emission maxima are usually associated with a drastic change in the excited state charge distribution as compared to that in the ground state. The excited state often has ICT or twisted ICT (TICT) character.[35,49] In a more polar solvent, the species with charge separation (ICT state) may become the lowest energy state. In a nonpolar solvent, the species without charge separation, the so-called locally excited (LE) state, may have the lowest energy, which can be ascribed to the benzoxazole chromophore. In this way, the role of the solvent polarity is not only to lower the energy of the excited state due to general solvent effects, but also to govern which state has the lowest energy.[50] It is worth observing that the fluorescence emission curve in the less polar solvent 1,4-dioxane seems broader in relation to the additional curves in Figure 9, probably indicating that the LE (~420 nm) and the ICT (484 nm) states are present in this solvent.[35]

Figure 5b depicts the emission curves to the dye **5b** using SW (340−351 nm) as the excitation wavelength. Only in dichloromethane can a clear dual fluorescence emission be observed with a main band located at 494 nm ascribed to the ICT state and the blue-shifted one related to an LE state (345 nm). In 1,4-dioxane, absolute ethanol, and acetonitrile, the emission band in the SW region mainly originates from the LE state. This result probably indicates that an inadequate geometry (twisted geometry) is present in these solvents, which are not able to present the ICT state.

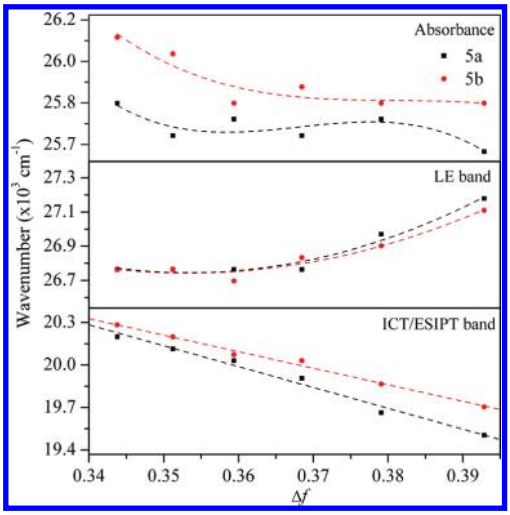

Figure 6. Solvent effect on the spectral position of the absorption maximum (top), and of the two fluorescence bands, SW (middle) and LW (bottom) for the Schiff bases **5a**,**b**. The Lippert−Mataga solvent polarity function Δf is given in eq 4.

The non-ESIPT dye **5b** demonstrates evidence of internal charge transfer (TICT or ICT) in the excited state. In order to correlate for mixed solvents the solvatochromic shifts with the solvent polarities, the dielectric constant (ε_{mix}) and the refractive index (n_{mix}) were calculated as already presented in the literature:[50,52]

$$\varepsilon_{mix} = f_A\varepsilon_A + f_B\varepsilon_B \quad (1)$$

$$n_{mix}^2 = f_A n_A^2 + f_B n_B^2 \quad (2)$$

where f_A and f_B are the volumetric fractions of the two solvents. On the basis of the assumption that a point dipole is situated at the center of the spherical cavity and neglecting the mean solute polarizability (α) in the states involved in the transition

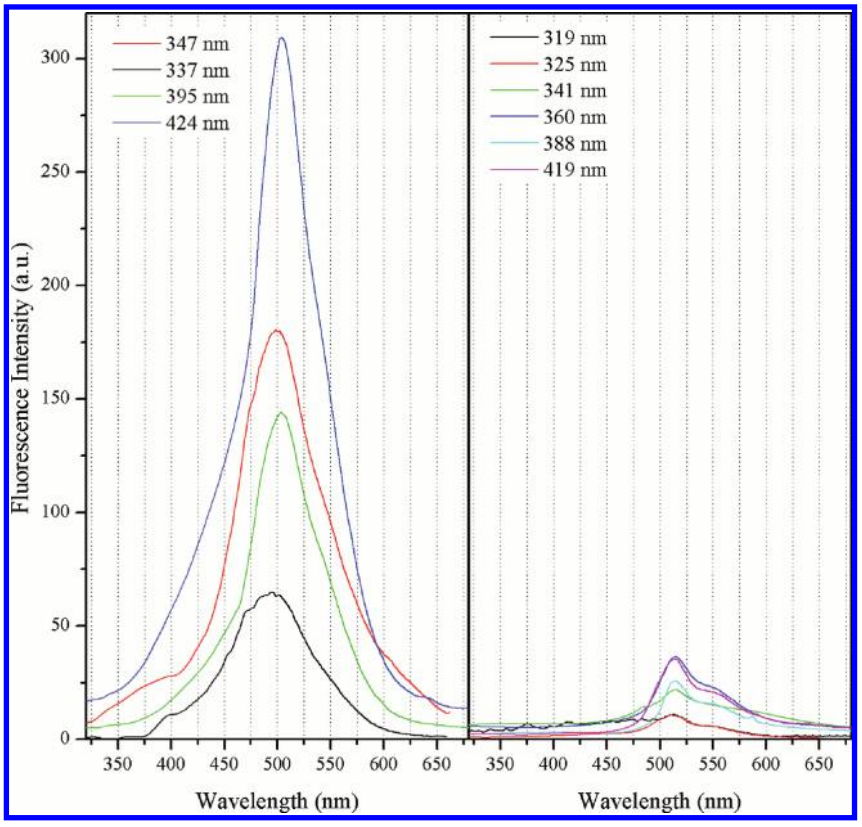

Figure 7. Fluorescence emission spectra for the dyes **5a** (left) and **5b** (right) in mineral oil Nujol. The two sets of curves are in the same Y axis scale.

($\alpha = \alpha_e = \alpha_g = 0$, where e and g stand for excited and ground states, respectively), one obtains[48,51]

$$h c \nu_{max} = h c \nu_{max}(0) - [2\mu_e(\mu_e - \mu_g)/a^3] \cdot \Delta f \quad (3)$$

$$\Delta f = f(\varepsilon) - (1/2) f(n) \quad (4)$$

$$f(\varepsilon) = (\varepsilon - 1)/(2\varepsilon + 1); \quad f(n) = (n^2 - 1)(2n^2 + 1) \quad (5)$$

where μ_g is the dipole moment of the solute in the ground state, ν_{max} is the solvent-equilibrated fluorescence maxima, $\nu_{max}(0)$ is the value of spectral position of the fluorescence maxima extrapolated to the gas phase, and a is the radius of the cavity in which the dye resides. It is worth mentioning that alcohols are usually excluded from these correlations to avoid specific solute−solvent interactions. Since charge transfer states can be more stabilized, increasing the solvent polarity, a linear relation of the fluorescence maxima (ν_{max}) versus the solvent polarity function (Δf) indicates the occurrence of the ICT state. It can be observed in Figure 6 that only the ICT/ESIPT bands show a linear fit ($r^2 = 0.99$ and 0.98 to the **5a**,**b**, respectively) of the fluorescence maxima versus the solvent polarity function, which can be related to the ICT state. Regarding the molecular structure of the dyes **5a**,**b**, the observed linearity seems to arise from a different mechanism in the excited state. For the dye **5b**, the ICT state arises from the push−pull character of the end groups presented in this structure.[49] On the other hand, the charge transfer character observed in ESIPT dyes generates a zwitterionic species in the excited state, as already discussed in similar dyes.[53−56] In this way, we believe that the ICT/ESIPT graphs are presenting the same interpretation: charge transfer, but from different pathways: electron delocalization (**5b**) and ESIPT mechanism (**5a**). The same linearity could not be observed for the absorption and LE bands in relation to the solvent polarity function, since these species are less polar than the ICT/ESIPT species.

Table 4. Calculated Properties of Schiff Bases in Ground and Excited Electronic States

	conformers		
calculated parameters	**5a**(enol)	**5a**(keto)	**5b**
	Ground State		
dipole moment (debye)	6.8531		7.8923
torsion angle[a] (degree)	42.3464		39.8063
Onsager radius (ångström)	5.34		5.30
	Excited State		
dipole moment (debye)	26.4531	17.1239	24.8199
torsion angle[a] (degree)	40.7939	30.7233	36.8968

[a] Dihedral angle between the atoms indicated in structure "a" of Figure 8.

Although there seems to be a lack of agreement in the need of the twisting to reach some ICT states, a simple experiment could lead us to observe this state in these compounds. It is well-known that viscosity can have a dramatic effect on the emission intensity of the dye. An example can be observed in the *trans*-stilbene, where the decrease of the fluorescence intensity can be interpreted as due to rotation about the central ethylene double bond in the excited state, which is thought to affect the emission of many other dyes.[57−60] Increase in local viscosity contributes to

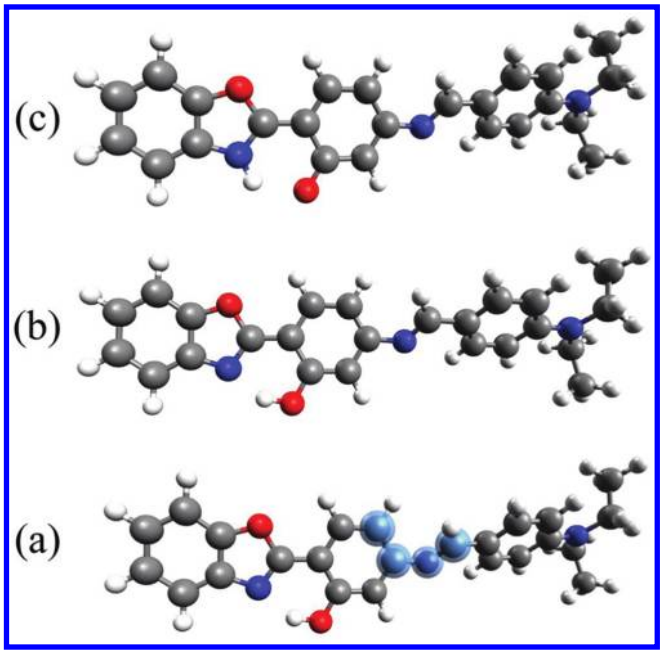

Figure 8. Structure of the Schiff base **5a**, where structure "a" is the enol conformer in the ground state and "b" and "c" are the enol conformer and the keto tautomer in the excited state, respectively.

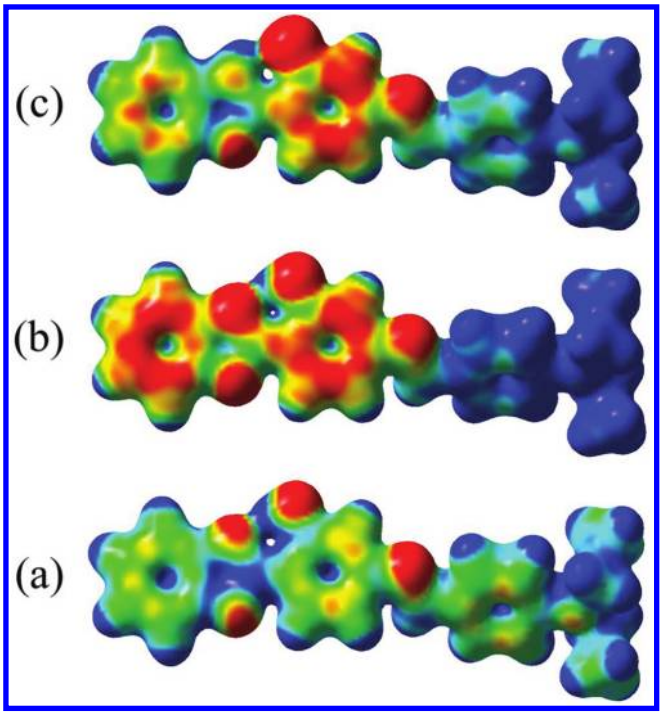

Figure 9. Electrostatic potential surfaces of the Schiff base **5a**, where structure "a" is the enol conformer in the ground state, and "b" and "c" are the enol conformer and the keto tautomer in the excited state, respectively. The most negative (electron-rich) potential is colored red, and the most positive (electron-poor) is colored blue.

the increased intensities displayed by many dyes when bound to biomolecules. However, when a twisting motion is needed to achieve an ICT state, the increase of the viscosity leads to a decrease of the fluorescence intensity, since the TICT produces a fluorescence quantum yield dependent on the surrounding environment.[35] In this way, additional fluorescence emission spectra were performed for two solutions of the dyes **5a,b**, in the same concentration, in mineral oil (Nujol) (viscosity 211 cP) (Figure 7).[61,62] It can be observed that only the fluorescence intensity from the dye **5b** is affected by the increase of the viscosity, as expected when a TICT state takes place in the excited state. This evidence leads us to conclude that the TICT state is formed upon the LE state of the dye **5b**.

Theoretical Calculations. The theoretical calculations indicate particular results concerning the planarity and electronic distribution of the Schiff bases. The most stable conformation for each species, both in the ground and excited state, is a nonplanar one, with torsion between the phenylbenzazolic chromophore and the diethylamino ring ranging from 30° to 42° (Table 4). These results are consistent with the experimental observation from the UV−vis spectra, where a less planar chromophore (C_a in Figure 3) absorbs radiation at the lower wavelengths. Figure 8 presents the optimized geometries corresponding to the Schiff base **5a**. Although the dye **5b** does not present the ESIPT mechanism, which excludes a keto tautomer in the excited state, a similar result could be obtained for the ground and excited states (Figures SI 23−24 in the Supporting Information).

The dipole moments of each species could also be calculated, where the structures in the excited state present a higher dipole moment in comparison to the ground state. These results are once again consistent with the experimental observation, since these dyes presented a positive solvatochromic effect when the polarity of the solvents is increased. Figure 9 depicts the electrostatic potential surfaces of Schiff base **5a** in the ground and excited states, which provides a means of visualizing this large increase in charge separation when these molecules are electronically excited. It is worth mentioning that the dye **5a** shows ESIPT in the excited state and also a linear plot of the fluorescence maxima versus the solvent polarity, indicating an unusually polar structure related to the ESIPT. Once again, the calculations reveal a charge separation in the excited state for the keto tautomer, as expected for this dye. A similar result could be obtained for **5b** in the ground and excited states (Figures SI 25 and 26 in the Supporting Information).

CONCLUSIONS

Two Schiff bases (**5a,b**) were synthesized by reaction of 2-(4′-aminophenyl)benzoxazoles derivatives with 4-*N*,*N*-diethylaminobenzaldehyde and fully characterized by means of infrared, ^{13}C and ^{1}H NMR, and elemental analysis. UV−vis and steady-state fluorescence in solution were also applied in order to characterize its photophysical behavior. These Schiff bases present absorption in the UV region (∼388 nm) with fluorescence emission in the blue-green region, with a large Stokes shift. The equilibrium between conformers in solution in the ground state, confirmed by the moderate solvatochromic effect due to two different conjugation lengths, reflects the dual fluorescence emission presented by these dyes. The fluorescence emission from the Schiff bases arises from different decay pathways. For the dye **5a**, an intramolecular proton transfer mechanism (ESIPT) mechanism may take place, where the emission at LW is related to the ESIPT mechanism, and the blue-shifted ones are due to conformational forms with a normal relaxation. On the other hand, a TICT is observed for the dye **5b**. Theoretical calculations show, consistently with experiment, that the most stable conformation of each species, both in the ground and

excited states, is nonplanar, and that the charge separation is much larger in the excited state when compared to the ground state.

■ ASSOCIATED CONTENT

Supporting Information. Original data from the spectroscopic characterization (FTIR, ^{1}H and ^{13}C NMR, and EI-MS), a general scheme of the ESIPT mechanism, the photophysical behavior of the precursors, and additional figures from the theoretical calculations. This material is available free of charge via the Internet at http://pubs.acs.org.

■ AUTHOR INFORMATION

Corresponding Author

*Phone: +55 51 3308 7176. Fax: +55 51 3308 7304. E-mails rodembusch@iq.ufrgs.br (F.S.R.); benvenutti@iq.ufrgs.br (E.V.B.).

■ ACKNOWLEDGMENT

We are grateful for financial support and scholarships from the Brazilian agencies CNPq and CAPES and Instituto Nacional de Inovação em Diagnósticos para a Saúde Pública (INDI-Saúde).

■ REFERENCES

(1) Armaroli, N.; Balzani, V. *Angew. Chem., Int. Ed.* **2007**, *46*, 52–66.
(2) Friedlingstein, P. *Nature* **2008**, *451*, 297–298.
(3) Grätzel, M. *Nature* **2001**, *414*, 338–344.
(4) World Energy Council. 2010 Survey of Energy Resources; http://www.worldenergy.org/publications/3040.asp (accessed October 4, 2010).
(5) Fujishima, A.; Honda, K. *Nature* **1972**, *238*, 37–38.
(6) Tributsch, H.; Pohlmann, L. *Science* **1998**, *279*, 1891–1895.
(7) Gerischer, H. *Electrochim. Acta* **1990**, *35*, 1677–1699.
(8) Hagfeldt, A.; Boschloo, G.; Sun, L.; Kloo, L.; Pettersson, H. *Chem. Rev.* **2010**, *110*, 6595–6663.
(9) O'Reagan, B.; Grätzel, M. *Nature* **1991**, *353*, 737–740.
(10) Nazeeruddin, M. K.; Kay, A.; Rodicio, I.; Humphry-Baker, R.; Muller, E.; Liska, P.; Vlachopoulos, N.; Grätzel, M. *J. Am. Chem. Soc.* **1993**, *115*, 6382–6390.
(11) Kay, A.; Grätzel, M. *Sol. Energy Mater. Sol. Cells* **1996**, *44*, 99–117.
(12) Bonhôte, P.; Gogniat, E.; Campus, F.; Walder, L.; Grätzel, M. *Displays* **1999**, *20*, 137–144.
(13) Tachibana, Y.; Moser, J. E.; Grätzel, M.; Klug, D. R.; Durrant, J. R. *J. Phys. Chem.* **1996**, *100*, 20056–20062.
(14) Kim, D.; Song, K.; Kang, M.-S.; Lee, J.-W.; Kang, S. O.; Ko, J. *J. Photochem. Photobiol., A: Chem.* **2009**, *201*, 102–110.
(15) Baik, C.; Kim, D.; Kang, M.-S.; Kang, S. O.; Ko, J.; Nazeeruddin, M. K.; Grätzel, M. *J. Photochem. Photobiol. A Chem.* **2009**, *201*, 168–174.
(16) Alloway, D. M.; Armstrong, N. R. *Appl. Phys. A: Mater. Sci. Process.* **2009**, *95*, 209–218.
(17) Ohmori, Y.; Itoh, E.; Miyairi, K. *Thin Solid Films* **2006**, *499*, 369–373.
(18) Ismail, Y. A. M.; Soga, T.; Jimbo, T. *Sol. Energy Mater. Sol. Cells* **2010**, *94*, 1406–1411.
(19) Ismail, Y. A. M.; Soga, T.; Jimbo, T. *Jap. J. Appl. Phys.* **2010**, *49*, 052301/1–052301/7.
(20) Wong, B. M.; Cordaro, J. G. *J. Chem. Phys.* **2008**, *129*, 214703/1–214703/8.
(21) Kulinich, A. V.; Ishchenko, A. A. *Russ. Chem. Rev.* **2009**, *78*, 141–164.
(22) Buerckstummer, H.; Kronenberg, N. M.; Meerholz, K.; Wuerthner, F. *Org. Lett.* **2010**, *12*, 3666–3669.
(23) Buerckstuemmer, H.; Kronenberg, N. M.; Gsaenger, M.; Stolte, M.; Meerholz, K.; Wuerthner, F. *J. Mater. Chem.* **2010**, *20*, 240–243.
(24) Kronenberg, N. M.; Deppisch, M.; Wuerthner, F.; Lademann, H. W. A.; Deing, K.; Meerholz, K. *Chem. Commun* **2008**, *48*, 6489–6491.
(25) Kronenberg, N. M.; Steinmann, V.; Buerckstuemmer, H.; Hwang, J.; Hertel, D.; Wuerthner, F.; Meerholz, K. *Adv. Mater.* **2010**, *22*, 4193–4197.
(26) Seo, J.; Kim, S.; Park, S. Y. *J. Am. Chem. Soc.* **2004**, *126*, 11154–11155.
(27) Santra, S.; Dogra, S. K. *Chem. Phys.* **1998**, *226*, 285–296.
(28) Rodembusch, F. S.; Campo, L. F.; Leusin, F. P.; Stefani, V. *J. Lumin.* **2007**, *126*, 728–734.
(29) Hillebrand, S.; Segala, M.; Buckup, T.; Correia, R. R. B.; Horowitz, F.; Stefani, V. *Chem. Phys.* **2001**, *273*, 1–10.
(30) Etaiw, S. E.-D. H.; Fayed, T. A.; Saleh, N. Z. *J. Photochem. Photobiol., A: Chem.* **2006**, *177*, 238–247.
(31) Fayed, T. A.; Etaiw, S. E.-D. H.; Khatab, H. M. *J. Photochem. Photobiol., A: Chem.* **2005**, *170*, 97–103.
(32) Fayed, T. A.; Ali, S. S. *Spectrosc. Lett.* **2003**, *36*, 375–386.
(33) Rettig, W. *Angew. Chem., Int. Ed. Engl.* **1996**, *25*, 971–988.
(34) Yoshihara, T.; Druzhinin, S. I.; Zachariasse, K. A. *J. Am. Chem. Soc.* **2004**, *126*, 8535–8539.
(35) Grabowski, Z. R.; Rotkiewicz, K.; Rettig, W. *Chem. Rev.* **2003**, *103*, 3899–4031.
(36) Lippert, E.; Lüder, W.; Moll, F.; Nägele, W.; Boos, H.; Prigge, H.; Seinbold-Blankenstein, I. *Angew. Chem.* **1961**, *73*, 695–706.
(37) Neese, F.; Wennmohs, F.; Becker, U.; Ganyushin, D.; Hansen, A.; Liakos, D.; Kollmar, C.; Kossmann, S.; Petrenko, T.; Reimann, C.; et al. *Lehrstuhl für Theoretische Chemie*; Universität Bonn: Bonn, Germany, 2010.
(38) Frisch, M. J.; Trucks, G. W.; Schlegel, H. B.; Scuseria, G. E.; Robb, M. A.; Cheeseman, J. R.; Montgomery, Jr., J. A.; Vreven, T.; Kudin, K. N.; Burant, J. C.; et al. *Gaussian 03*; Gaussian, Inc.: Wallingford, CT, 2004.
(39) Barni, E.; Savarino, P.; Marzona, M.; Piva, M. *J. Heterocycl. Chem.* **1983**, *20*, 1517–1521.
(40) Rodembusch, F. S.; Leusin, F. P.; Bordignon, L. B.; Gallas, M. R.; Stefani, V. *J. Photochem. Photobiol., A: Chem.* **2005**, *173*, 81–92.
(41) Douhal, A.; Amat-Guerri, F.; Lillo, M. P.; Acuña, A. U. *J. Photochem. Photobiol., A: Chem.* **1994**, *78*, 127–138.
(42) Guallar, V.; Moreno, M.; Lluch, J. M.; Amat-Guerri, F.; Douhal, A. *J. Phys. Chem.* **1996**, *110*, 19789–19794.
(43) Nagaoka, S.-I.; Kusunoki, J.; Fujibuchi, T.; Hatakenaka, S.; Mukai, K.; Nagashima, U. *J. Photochem. Photobiol. A Chem.* **1999**, *122*, 151–195.
(44) Inagaki, T. *J. Chem. Phys.* **1972**, *57*, 2526–2530.
(45) Tchaikovskaya, O. N.; Sokolova, I. V.; Yudina, N. V. *Luminescence* **2005**, *20*, 187–191.
(46) Hammud, H. H.; Ghannoum, A.; Masoud, M. S. *Spectrochim. Acta, Part A* **2006**, *63*, 255–265.
(47) Forbes, W. F.; Leckie, I. R. *Can. J. Chem.* **1958**, *36*, 1371–1380.
(48) Nikolai, V. T. *Optical Spectroscopy: Methods and Instrumentations*, 1st ed.; Elsevier Science: Amsterdam, 2006; pp 115.
(49) Zachariasse, K. A.; Grobys, M.; von der Haar, T.; Hebecker, A.; Il'ichev, Y. V.; Jiang, Y. B.; Morawski, O.; Kühnle, W. *J. Photochem. Photobiol., A: Chem.* **1996**, *102*, 59–70.
(50) Lakowicz, J. R. Solvent and Environmental Effects. *Principles of Fluorescence Spectroscopy*, 3rd ed.; Springer: New York, 2006; pp 207.
(51) Singh, M. K.; Pal, H.; Bhasikuttan, A. C.; Sapre, A. V. *Photochem. Photobiol.* **1998**, *68*, 32–38.
(52) Bhasikuttan, A. C.; Palit, D. K.; Sapre, A. V.; Mittal, J. P. *Chem. Phys. Lett.* **2000**, *316*, 67–74.
(53) Ameer-Beg, S.; Ormson, S. M.; Brown, R. G.; Matousek, P.; Towrie, M.; Nibbering, E. T. J.; Foggi, P.; Neuwahl, F. V. R. *J. Phys. Chem. A* **2001**, *105*, 3709–3718.
(54) Brucker, G. A.; Swinney, T. C.; Kelley, D. F. *J. Phys. Chem.* **1991**, *95*, 3190–3195.
(55) Koll, A.; Filarowski, A.; Fitzmaurice, D.; Waghorne, E.; Mandal, A.; Mukherjee, S. *Spectrochim. Acta, Part A* **2002**, *58*, 197–207.

(56) Sahoo, D.; Adhikari, T.; Chowdhury, P.; Roy, S. C.; Chakravorti, S. *Chem. Phys.* **2008**, *352*, 175–184.
(57) Sumitani, M.; Nakashima, N.; Yoshihara, K.; Nagakura, S. *Chem. Phys. Lett.* **1977**, *51*, 183–185.
(58) Rettig, W.; Lapouyade, R. Fluorescence probes based on twisted intramolecular charge transfer (TICT) states and other adiabatic photoreactions. In *Topics in Fluorescence Spectroscopy: Probe Design and Chemical Sensing*, 1st ed.; Lakowicz, J. R., Ed.; Kluwer Academic Publishers: New York, 1994; Vol. 4, pp 109−149.
(59) Meier, H. *Angew. Chem., Int. Ed.* **2001**, *40*, 1851–1853.
(60) Todd, D. C.; Jean, J. M.; Rosenthal, S. J.; Ruggiero, A. J.; Yang, D.; Fleming, G. R. *J. Chem. Phys.* **1990**, *93*, 8658–8668.
(61) Bureš, F.; Pytela, O.; Kivala, M.; Diederich, F. *J. Phys. Org. Chem.* **2011**, *24*, 274–281.
(62) Sutharsan, J.; Lichlyter, D.; Wright, N. E.; Dakanali, M.; Haidekker, M. A.; Theodorakis, E. A. *Tetrahedron* **2010**, *66*, 2582–2588.